Supporting Information

Electrochemical Hole Injection Selectively Expels Iodide from Mixed Halide Perovskite Films

Gergely F. Samu,[1,2,3] Ádám Balog,[1] Filippo De Angelis,[4,5,6] Daniele Meggiolaro[4,5]

Prashant V. Kamat,[3,7,*] Csaba Janáky[1,2,*]

[1]Department of Physical Chemistry and Materials Science, Interdisciplinary Excellence Centre, University of Szeged, Rerrich Square 1, Szeged, H-6720, Hungary

[2]ELI-ALPS Research Institute, Szeged, Dugonics sq. 13, 6720, Hungary

[3]Department of Chemistry and Biochemistry, University of Notre Dame

[4] Department of Chemistry, Biology and Biotechnology, University of Perugia, Via Elce di Sotto 8I-06123, Perugia, Italy

[5] Computational Laboratory for Hybrid/Organic Photovoltaics (CLHYO), CNR-ISTM, Via Elce di Sotto 8, 06123, Perugia, Italy

[6] CompuNet, Istituto Italiano di Tecnologia, Via Morego 30, 16163 Genova, Italy

[7]Radiation Laboratory, University of Notre Dame, Notre Dame, Indiana, 46556, United States

Materials and Methods

Materials

Lead iodide (PbI_2, Alfa Aesar, Ultradry, beads, −10 mesh, 99.999% trace metals basis), lead bromide ($PbBr_2$, Alfa Aesar, Puratronic®, 99.998% trace metals basis), methylammonium iodide (MAI, Greatcellsolar), methylammonium bromide (MABr, Greatcellsolar), dimethyl sulfoxide (DMSO, Sigma-Aldrich, anhydrous, >99.9%), n,n-dimethyl-formamide (DMF, Sigma-Aldrich, anhydrous, 99.8%), diethyl ether (DEE, Sigma-Aldrich, for HPLC, ≥99.9%, inhibitor-free) were used for the synthesis of the mixed-halide perovskite electrodes without further purification.

Electrochemical experiments were carried out in dichloromethane (DCM, Sigma Aldrich, anhydrous, ≥99.8%, contains 40-150 ppm amylene as stabilizer, dried over 3Å molecular sieves) with tetrabutylammonium hexafluorophosphate (Bu_4NPF_6 – Sigma Aldrich, for electrochemical analysis, ≥99.0%) as the conducting electrolyte. Bu_4NPF_6 was dried prior to use in a vacuum oven at T=180 °C.

All solutions and electrodes were prepared in a glovebox (N_2 atmosphere, H_2O < 0.1 ppm, O_2 < 0.1 ppm).

Electrode preparation methods

The mixed halide perovskite electrodes were prepared by a one-step method, where all the precursors were dissolved in dimethylformamide, and subsequently spin-coated on FTO substrates. The FTO substrates were cleaned with soap, rinsed with DI water, sonicated in ethanol for 20 minutes and finally plasma-cleaned prior to use.

In the case of measurements were spectroscopic techniques were involved thin $MAPbBr_{1.5}I_{1.5}$ films were prepared. The spin coating solution consisted of 0.175 M PbI_2, $PbBr_2$, MaI, MaBr and 0.35 M DMSO in DMF. For XRD, ICP-OES and ion-chromatography thick $MAPbBr_{1.5}I_{1.5}$ films were prepared by increasing the precursor concentration to 1.4 M together with 1.4 M DMSO in DMF. Prior to spin coating the solutions were left to stir for 1 h at room temperature, and was filtered with an inorganic membrane filter (0.2 μm pore size, G8549141, Whatman) before use. During spin-coating the samples were subjected to an antisolvent treatment step with diethyl-ether. After the spin coating the samples were immediately transferred to a hot-plate (preheated at T=65 °C) for 1 min to ensure evaporation of the antisolvent. This was followed by an annealing step (at T=100 °C) for 2 min.

A one step static coating procedure was used on a 2.5 cm x 2.5 cm FTO substrate: (1) at 4000 rpm for 25 s. 50 μl of perovskite solution was used. 0.5 ml DEE was dispensed on the spinning substrate in a continuous motion in less than 4 s during the early stage (6 s elapsed time) of the film formation.

Electrochemical measurements

Electrochemical measurements were carried out with a Princeton Applied Research PARStat 2273 potentiostat in a standard three-electrode setup. The FTO/mixed halide perovskite electrodes functioned as the working electrode, a Pt mesh (1 cm^2) as the counterelectrode (cleaned by “Piranha solution”, water, and finally DCM), and a Ag/AgCl wire as a pseudoreference electrode. Calibration of the pseudoreference electrode was carried out by

measuring the formal potential of the ferrocene/ferrocenium redox couple in DCM (0.01 M ferrocene and 0.1 M Bu_4NPF_6). The formal potential was found to be E = 0.45 ± 0.04 V vs. our Ag/AgCl by analysis of cyclic voltammograms at various sweep rates. The electrochemical cells were assembled in a glovebox (N_2 atmosphere, H_2O < 0.1 ppm, O_2 < 0.1 ppm) and sealed to ensure inert conditions.

Electrochemical impedance spectroscopy

Electrochemical impedance spectroscopy measurements were performed with a Metrohm Autolab PGSTAT302 type potentiostat/galvanostat in a standard three-electrode setup. Full impedance spectra were recorded at different potential values in the 100 kHz to 0.1 Hz frequency range, using a sinusoidal excitation signal (10 mV RMS amplitude).

In situ Raman spectroelectrochemistry

Raman measurements were carried out by a SENTERRA II Compact Raman microscope, using 785 nm laser excitation wavelength with a laser power of 10 mW and a 50X objective. In situ Raman spectroelectrochemistry was performed using an ECC-Opto-Std electrochemical cell (EL-CELL GmbH) equipped with a sapphire window, and a potentiostat/galvanostat (DropSens μstat 400). The spectra were recorded after a 100 s potentiostatic conditioning at the given potential. As the working electrode in this specific setup is a platinum mesh, the layers were prepared by spray-coating. The same mixed halide perovskite precursor solution was used, as for the spin-coating. During the spray-coating the platinum mesh was placed on a hot plate preheated to 100 °C and kept there for 2 minutes after spray-coating.

Characterization methods

Steady state UV-vis absorption spectra and spectroelectrochemical measurements of the prepared electrodes, were recorded with a Cary 50 Bio spectrophotometer (Varian). Top-down scanning electron microscopic (SEM) images were captured using a FEI SEM Magellan 400 XHR instrument. X-ray diffraction (XRD) patterns were collected using a Bruker D8 DISCOVER instrument with Cu Kα X-ray source (λ = 1.5406 Å), in the 10−35° range, with a 2° min^{-1} scan rate. The characterization of surface chemistry of perovskite films was performed with a laboratory-based, ambient pressure X-ray photoelectron spectrometer with a monochromatic Al Kα X-ray source (1486.6 eV). All spectra were calibrated to their corresponding C 1s which is 285.3 eV.

To determine the composition of the electrodes, inductively-coupled plasma optical emission spectroscopy (ICP-OES) for lead and ion chromatography for halides were employed. The electrodes were digested from the FTO substrates in 10 ml of DI water via sonication for 30 minutes. 5 ml of the resulting solution was then used for ICP-OES and ion chromatography measurements. For the ICP-OES solutions nitric acid (HNO_3 BDH, 69-70%) was added to form a 2% HNO_3 solution. For the ICP-OES measurements a Perkin-Elmer Optima 8000 instrument was used. ICP elemental calibration curve for Pb^{2+} was recorded using commercial standards (Inorganic Ventures) in the 0.5 – 50 ppm concentration regime. The monitored emission wavelength for Pb^{2+} was 220.353 nm. For the Br^- and I^- concentration determination a Dionex ICS-5000 system equipped with a Dionex IonPac AS14A column along with an AG14A guard was used. Calibration curves for Br^-/I^- were recorded using commercial standards (Inorganic Ventures) in the 0.5 – 30 ppm concentration regime. The mobile phase for all ion chromatography measurements was an 8 mM carbonate/1 mM bicarbonate solution in DI water.

Transient absorption spectroscopy

A Clark MXR-2010 laser system (775 nm fundamental, 1 mJ/pulse, FWHM=150 fs, 1 kHz repetition rate) was used to perform the ultrafast transient spectroscopy measurements. The data was collected using a Helios software from Ultrafast Systems. The fundamental was separated in an intensity ratio of 95/5, where the 95% was doubled in frequency to generate the 387 nm excitation pump. The remaining 5% was used to generate a white light continuum via a CaF_2 crystal. This light was used as the probe for all measurements. A pump excitation of about 4 μJ cm^{-2} was used in all measurements.

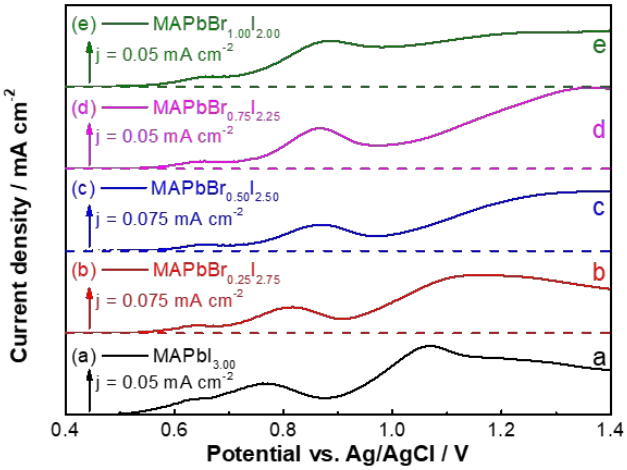

Figure S1. Linear sweep voltammograms of FTO/$MAPbBr_xI_{3-x}$ electrodes in 0.1 M Bu_4NPF_6/DCM electrolyte (5 mV s^{-1} sweep rate).

Table S1. Summary of peak potentials and peak currents of FTO/$MAPbBr_xI_{3-x}$ electrodes from linear sweep voltammograms in 0.1 M Bu_4NPF_6/DCM electrolyte (5 mV s^{-1} sweep rate).

	Wave 1 – pre-peak		Wave 2 - sharp peak		Peak current ratio – j_2/j_1
Material	Peak potential / V	Peak current density / mA cm^{-2}	Peak potential / V	Peak current density / mA cm^{-2}	
$MAPbI_3$	0.62	0.019	0.77	0.038	2.0
$MAPbBr_{0.25}I_{2.75}$	0.64	0.014	0.81	0.047	3.4
$MAPbBr_{0.50}I_{2.50}$	0.66	0.011	0.86	0.048	4.4
$MAPbBr_{0.75}I_{2.25}$	0.67	0.009	0.86	0.049	5.4
$MAPbBr_{1.00}I_{2.00}$	0.66	0.012	0.88	0.056	4.7
$MAPbBr_{1.50}I_{1.50}$	0.66	0.011	0.9	0.043	3.9
$MAPbBr_{2.25}I_{0.75}$	~0.7	~0.009	0.84	0.028	3.1
$MAPbBr_3$	~1.0	~0.009	1.15	0.04	4.4

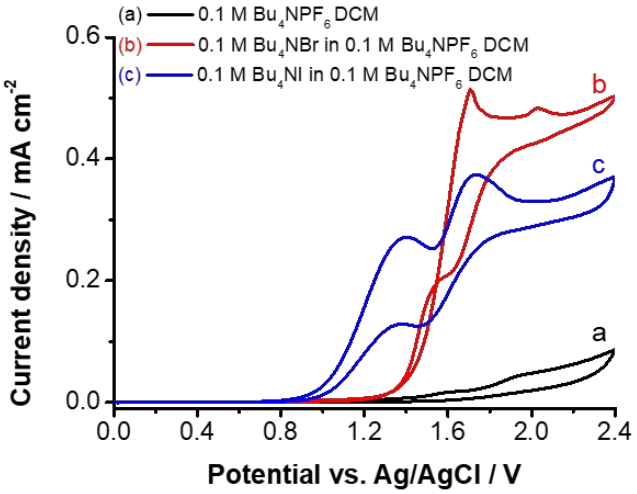

Figure S2. Cyclic voltammograms recorded on FTO electrodes for 0.1 M Bu_4NBr and Bu_4NI containing 0.1 M Bu_4NPF_6/DCM electrolyte (5 mV s^{-1} sweep rate).

Electrochemical impedance spectroscopy

The electronic properties of MHP layers are also influenced by their composition as shown by electrochemical impedance spectroscopy (EIS) (**Fig. S3**). In the case of $MAPbBr_{1.5}I_{1.5}$ films different behavior can be observed in the #1 (**Fig. S3A**) and #2 (**Fig. S3B**) region of the linear sweep voltammograms (LSVs). Qualitatively in the #1 region of the LSV (between 0.6 V – 0.7 V) the Nyquist plots can be described by an initial semicircle at high frequencies followed by an ideal Warburg impedance. As the potential is increased in this region the decrease in the size of the semicircle signals the decrease in the charge transfer resistance (R_{CT}) of the films. As hole trapping occurs on the iodide site in the perovskite material, the transfer of electrons from the solution to the $MAPbBr_{1.5}I_{1.5}$ becomes more favorable (less electron density near the valence band), thus the decrease in the R_{CT} of the films is observed. This trapping induces iodide migration in the film, which is indicated by the perfect slope (near 45°) of the Warburg impedance at low frequencies. As the potential is further increased (#2 region on the LSV between 0.7 V – 1.0 V) a markedly different behavior is observed. The increase in the size of the semicircle at high frequencies is seen, which translates to an increase in the R_{CT} of the films. As hole injection to the valence band of $MAPbBr_{1.5}I_{1.5}$ occurs in this potential region, the iodide (and possibly MA) is gradually expelled into the solution. The increase in the R_{CT} value reflects this gradual conversion of the film into pure $MAPbBr_3$ (**Fig. S3C**). Furthermore, a distorted Warburg behavior at low frequencies is observed, which can be related to the anomalous (mixed) diffusion observed in this regime.[1,2] Note, that behavior of $MAPbBr_3$ (**Fig. S3C**) correlates well with the initial behavior of the MHP (decreasing R_{CT} with increasing potential), without the movement of iodide in the lattice (missing Warburg impedance at low

frequencies). The same layer was subjected to a further cycle of EIS measurements. Interestingly after the EIS measurements the full conversion to $MAPbBr_3$ was not achieved, however a strikingly similar behavior to an iodide poor perovskite $MAPbBr_{2.25}I_{0.75}$ was observed (**Fig. S3D**). Furthermore, EIS reveals that MHPs possess superior electronic properties compared to pure $MAPbBr_3$ as they exhibit smaller R_{CT}.

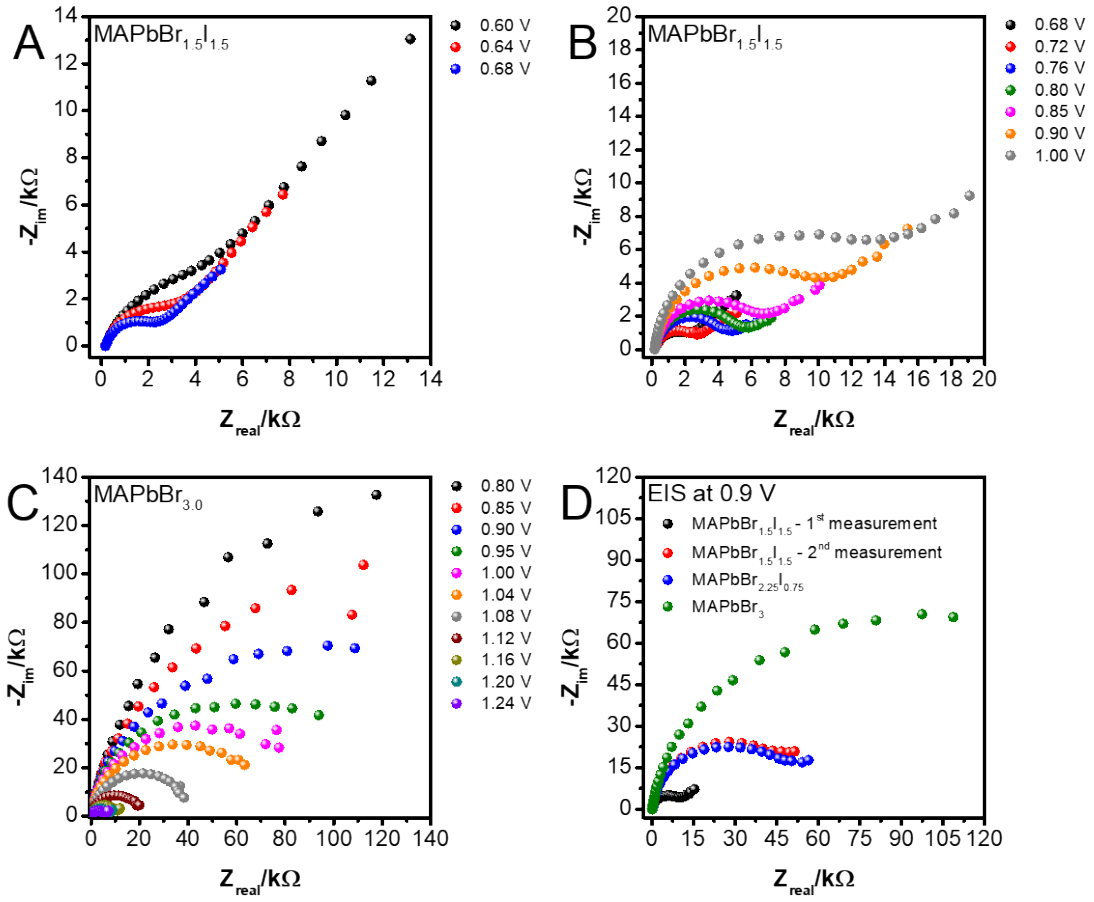

Figure S3. Nyquist plots from electrochemical impedance spectroscopic measurements at different potentials **A:** for FTO/$MAPbBr_{1.5}I_{1.5}$ electrodes in the #1 region of the LSV, **B:** for FTO/$MAPbBr_{1.5}I_{1.5}$ electrodes in the #2 region of the LSV, and **C:** FTO/$MAPbBr_{3.0}$ recorded in the full potential range in 0.1 mol dm^{-3} Bu_4NPF_6/DCM electrolyte. **D:** Comparison of Nyquist plots for different FTO/perovskite electrodes at 0.9 V vs. Ag/AgCl.

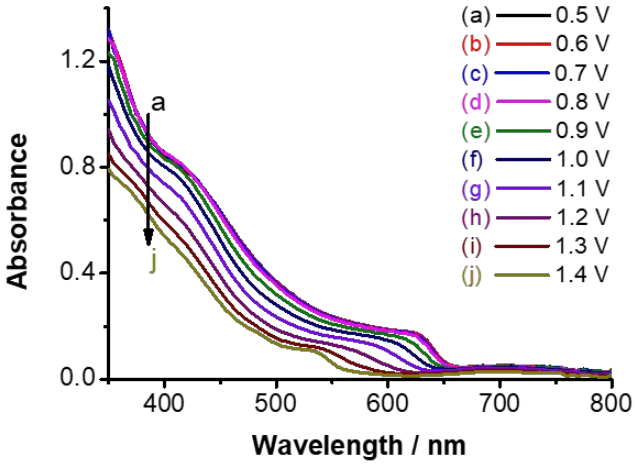

Figure S4. UV-vis spectra of FTO/$MAPbBr_{1.5}I_{1.5}$ films recorded between 0.5 V and – 1.4 V (vs. Ag/AgCl) during potentiodynamic cycling in 0.1 M Bu_4NPF_6/DCM electrolyte (5 mV s^{-1} sweep rate).

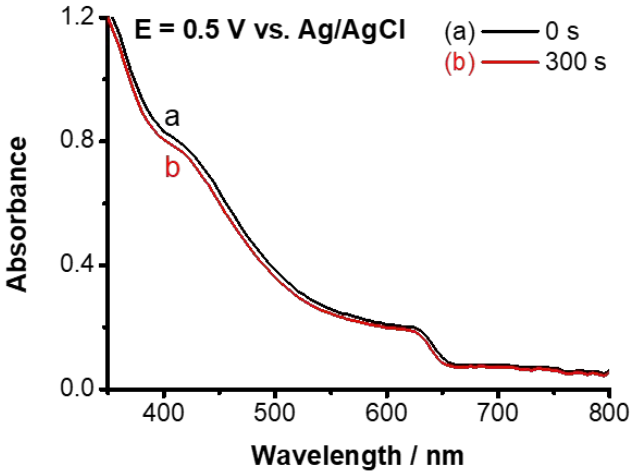

Figure S5. UV-vis absorbance spectra of FTO/$MAPbBr_{1.5}I_{1.5}$ films in 0.1 M Bu_4NPF_6/DCM electrolyte before and after potentiostatic treatment at 0.5 V vs. Ag/AgCl for 300 s.

In situ Raman spectroelectrochemistry

To further monitor the underlying structural changes of the films during the iodide expulsion process, *in situ* Raman spectroelectrochemistry measurements were performed **(Fig. S6-S8)**. The untreated MHP films show characteristic Raman modes identical to literature data **(Fig. S6).**[3] Most of these modes are related to vibrations of the methylammonium-cation in the perovskite lattice. When electrochemical bias is applied, no change in these modes was observed. Which translates to the fact that at least a portion of MA remains in the perovskite lattice. Notably, as the applied electrochemical bias was increased until the point, where iodide migration starts in the film, a broad fluorescence signal was observed **(Fig. S7B)**. As $MAPbI_3$ is the only species capable of absorbing the exciting laser light (λ = 780 nm) and subsequently

emitting light, this further proves the first step of the expulsion process is the formation of iodide-rich domains in the films. When the actual iodide expulsion event occurs from the MHP films, the decrease of the fluorescence from the iodide rich domains was observed **(Fig. S7C)**. After this additional Raman-features emerge, which can be possibly caused by the presence of PbI_2, the intermediate of the expulsion process. This alteration is also observable in the color change of the MHP films, which are presented on the Raman microscopic images **(Fig. S7)**. Interestingly, the iodide rich domain formation (before the iodide expulsion event) can be reversed. The initial Raman-features of the MHP films can be restored through leaving the films to relax in the dark **(Fig. S8A)**, or by the application of an external reverse bias to expedite the process **(Fig. S8B)**. This shows the reversibility of the phase segregation process (even in the presence of the electrolyte) until the iodide expulsion event occurs.

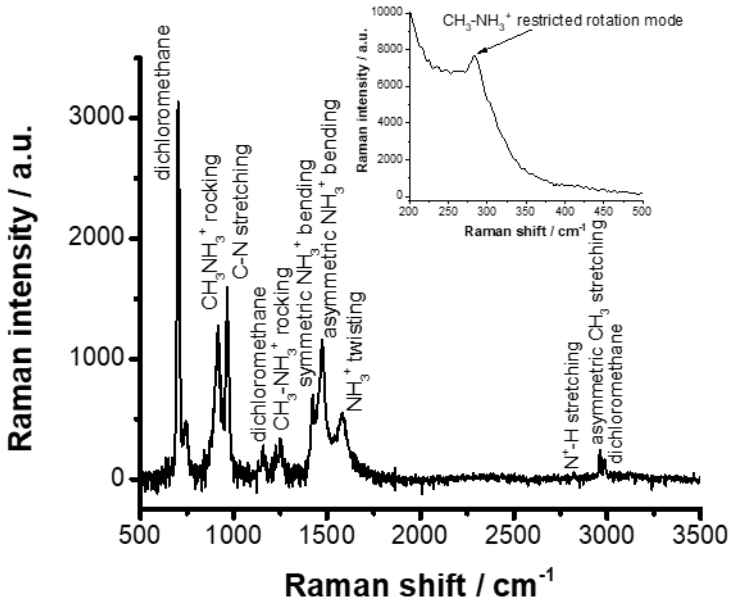

Figure S6. In situ Raman spectroelectrochemistry of spray coated $MAPbBr_{1.5}I_{1.5}$ films on a Pt mesh in 0.1 M Bu_4NPF_6/DCM electrolyte under open circuit conditions.

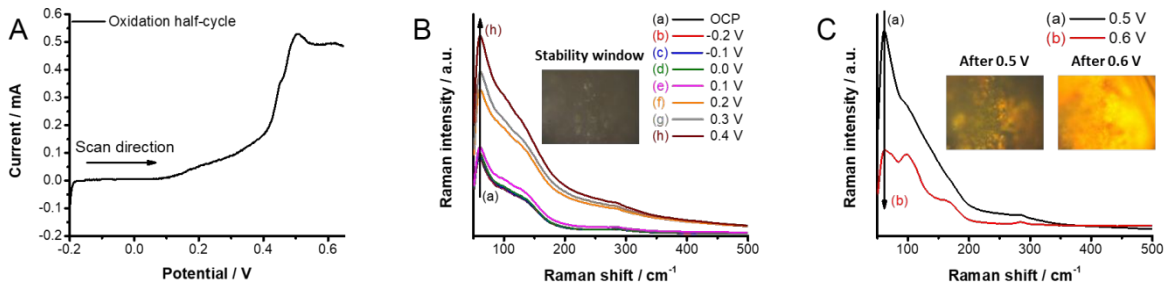

Figure S7. A: Linear sweep voltammogram of the spray coated $MAPbBr_{1.5}I_{1.5}$ films on a Pt mesh in 0.1 M Bu_4NPF_6/DCM electrolyte with a sweep rate of 2 mV s^{-1}. Potentiostatic Raman spectroelectrochemistry of spray coated $MAPbBr_{1.5}I_{1.5}$ films on a Pt mesh in 0.1 M Bu_4NPF_6/DCM electrolyte, together with microscopic images **B:** within the stability window, **C:** out of the stability window.

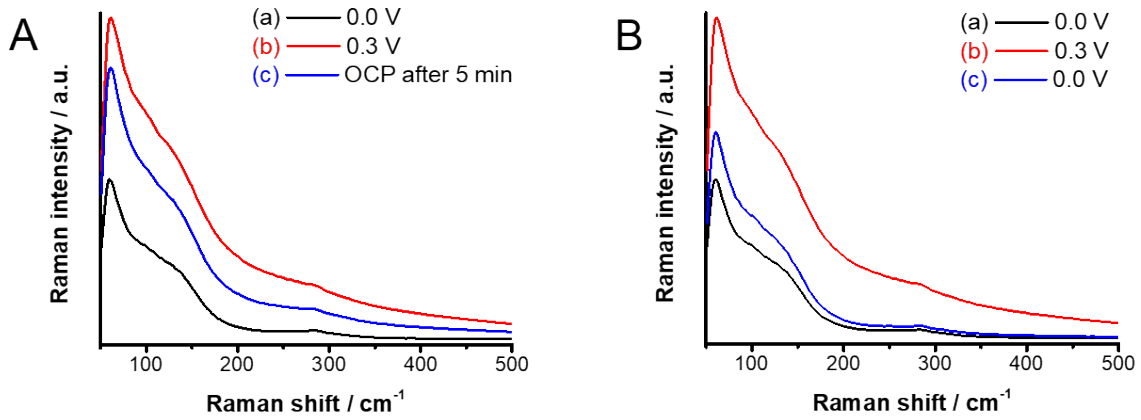

Figure S8. Relaxation of the fluorescence background during Raman spectroelectrochemistry measurements of the spray coated $MAPbBr_{1.5}I_{1.5}$ films on a Pt mesh in 0.1 M Bu_4NPF_6/DCM electrolyte **A:** The effect of 5 minute relaxation in the dark and **B:** The effect of 1 minute potentiostatic treatment at 0.0 V.

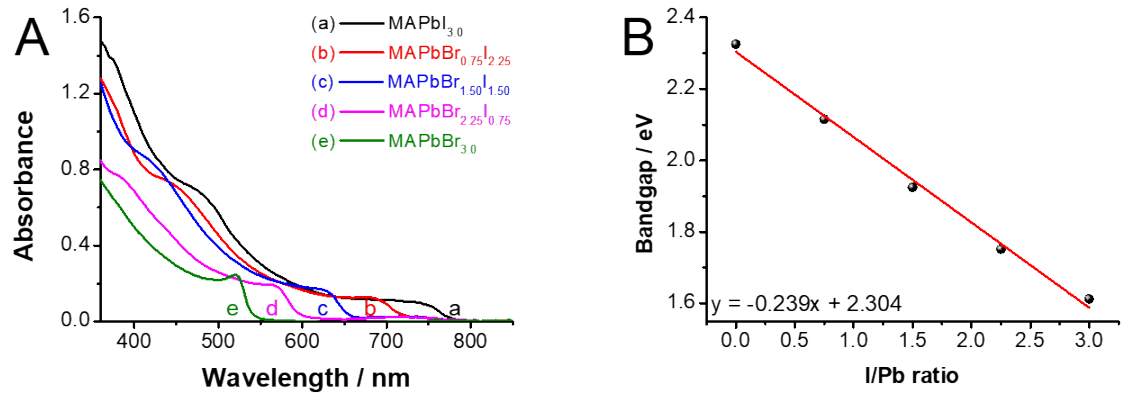

Figure S9. A: UV-vis absorption spectra of FTO/$MAPbBr_xI_{3-x}$ electrodes in 0.1 M Bu_4NPF_6/DCM electrolyte. **B:** The determined bandgap from the derived Tauc plots as the function of theoretical composition (I/Pb ratio).

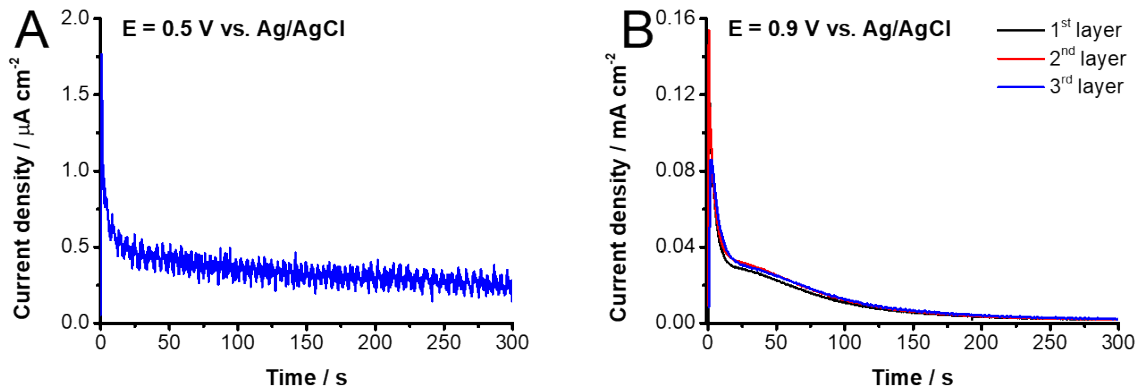

Figure S10. Chronoamperometric curves of FTO/$MAPbBr_{1.5}I_{1.5}$ electrodes in 0.1 M Bu_4NPF_6/DCM electrolyte recorded at **A:** 0.5 V vs. Ag/AgCl, and **B:** 0.9 V vs. Ag/AgCl potentials.

Compositional analysis

Table S2. Experimentally determined surface composition of FTO/$MAPbBr_{1.5}I_{1.5}$ electrodes before and after potentiostatic treatment from X-ray photoelectron spectroscopy measurements. The standard deviation of the compositions was derived from 3 separate measurements.

		Pb^{2+}	Pb^{0}	Br	I	N
As-is $MAPbBr_{1.5}I_{1.5}$	Average / at%	18.6	0	26.6	38.3	16.5
	Normalized to Pb^{2+}	1	0	1.43	2.06	0.89
Middle composition (E=0.9 V vs. Ag/AgCl t=30s)	Average / at%	25.0 ± 0.3	0	15.4 ± 0.4	51.6 ± 0.9	8.0 ± 0.9
	Normalized to Pb^{2+}	1 ± 0.01	0	0.61 ± 0.01	2.06 ± 0.04	0.32 ± 0.03
Final composition (E=0.9 V vs. Ag/AgCl t=300s)	Average / at%	28.5 ± 0.8	2.3 ± 0.1	37.4 ± 0.1	26.7 ± 3.3	8.3 ± 1.5
	Normalized to Pb^{2+}	1 ± 0.03	0.08 ± 0.01	1.31 ± 0.01	0.94 ± 0.12	0.29 ± 0.05

Table S3. Experimentally determined composition of FTO/$MAPbBr_{1.5}I_{1.5}$ electrodes before and after potentiostatic treatment from energy dispersive spectroscopy (EDX) measurements. The standard deviation of the compositions was derived from 3 separate measurements.

		Pb	Br	I
As-is $MAPbBr_{1.5}I_{1.5}$	Average / at%	21.3 ± 0.3	40.8 ± 0.5	37.9 ± 0.9
	Normalized to Pb	1.0 ± 0.01	1.92 ± 0.02	1.78 ± 0.05
Middle composition (E=0.9 V vs. Ag/AgCl t=30s)	Average / at%	26.2 ± 1.6	48.5 ± 4.3	25.3 ± 3.2
	Normalized to Pb	1.0 ± 0.06	1.85 ± 0.17	0.97 ± 0.12
Final composition (E=0.9 V vs. Ag/AgCl t=300s)	Average / at%	27.9 ± 0.0	53.5 ± 2.3	18.6 ± 0.9
	Normalized to Pb	1.0 ± 0.00	1.92 ± 0.08	0.67 ± 0.03

Table S4. Experimentally determined composition of thick FTO/$MAPbBr_{1.5}I_{1.5}$ electrodes before and after potentiostatic treatment from analytical measurements. The Pb^{2+} content was determined from ICP-OES, while the Br^- and I^- content was determined from ion chromatography. The standard deviation of the compositions was derived from 2 separate electrodes.

		Pb^{2+}	Br^-	I^-
as-is $MAPbBr_{1.5}I_{1.5}$	Amount/ µmol	32.6 ± 0.2	58.0 ± 0.1	57.6 ± 0.6
	Lead normalized amount	1.00 ± 0.01	1.78 ± 0.01	1.77 ± 0.02
Middle composition (E=0.9 V vs. Ag/AgCl t=30s)	Amount / µmol	29.9 ± 0.9	57.4 ± 3.7	39.0 ± 5.8
	Lead normalized amount	1.00 ± 0.03	1.92 ± 0.12	1.30 ± 0.20
Final composition (E=0.9 V vs. Ag/AgCl t=300s)	Amount / µmol	30.1 ± 2.7	58.4 ± 0.9	30.8 ± 0.02
	Lead normalized amount	1.00 ± 0.09	1.94 ± 0.03	1.02 ± 0.01

Summary of the compositions obtained from various techniques

Cross-comparison of the gathered data from the different analytical techniques was carried out and the results are shown in **Table S5**. The measured compositions were normalized with respect to the Pb content of the electrodes determined with the given technique. Pb could be used as an internal standard, as ICP-OES measurements carried out for the electrolyte shown only trace amounts of Pb in the electrolyte after prolonged potentiostatic treatment at 0.9 V vs. Ag/AgCl. Thus, it could be concluded that no Pb dissolution occurs during the iodide expulsion process. Note that when a given technique is not sensitive to MA, it is shown in parentheses.

Table S5. Experimentally determined compositions of FTO/$MAPbBr_{1.5}I_{1.5}$ electrodes from various analytical measurements, before and after potentiostatic treatment. All data were normalized with respect to the Pb content of the electrodes. In the case of XPS the composition shown in brackets takes into account a 1:1 stoichiometric relationship between the nitrogen and Pb content of MHPs.

Sample	UV-vis (from Fig. S6B)	UV-vis (from ref. 4)	EDX	ICP-OES + IC	XRD	XPS
$MAPbBr_{1.5}I_{1.5}$	$MAPbBr_{1.50}I_{1.50}$	$MAPbBr_{1.80}I_{1.20}$	$(MA)PbBr_{1.92}I_{1.78}$	$(MA)PbBr_{1.78}I_{1.77}$	$MAPbBr_{1.84}I_{1.16}$	$MA_{0.89}PbBr_{1.43}I_{2.06}$ [89% $MAPbBr_{1.61}I_{2.10}$ + 11% PbI_2]
Middle composition (E=0.9 V vs. Ag/AgCl t=30s)	$MAPbBr_{2.01}I_{0.99}$	$MAPbBr_{2.16}I_{0.84}$	$(MA)PbBr_{1.85}I_{0.97}$	$(MA)PbBr_{1.92}I_{1.30}$	$MAPbBr_{2.62}I_{0.38}$ + $MAPbBr_{2.29}I_{0.71}$	$MA_{0.32}PbBr_{0.61}I_{2.06}$ [32% $MAPbBr_{1.91}I_{2.19}$ + 68% PbI_2]
Final composition (E=0.9 V vs. Ag/AgCl t=300s)	$MAPbBr_{2.90}I_{0.10}$	$MAPbBr_{3.00}$	$(MA)PbBr_{1.92}I_{0.67}$	$(MA)PbBr_{1.94}I_{1.02}$	contracted $MAPbBr_{3.0}$ + $MAPbBr_{2.29}I_{0.71}$	$MA_{0.29}PbBr_{1.31}I_{0.94}$ [29% $MAPbBr_{2.86}$ + 47% PbI_2 + 24% $PbBr_2$]

Both EDX and ICP-OES + IC results show a constant bromide content of the electrodes even after the electrochemical treatment. As the potentiostatic treatment progresses in time, the iodide content of the electrodes gradually decreases from its initial value, which signals iodide expulsion from the electrodes to the electrolyte. Cross-relating these results with the composition acquired from the peak positions of the XRD patterns, a similar bromide content for the initial composition can be extracted. This signals that the excess iodide in the case of EDX and ICP-OES and IC measurements arises from the presence of mainly amorphous PbI_2 in the layers. As we perform the electrochemical treatment the MHP phase is enriched in bromide and the amount of iodide decreases. In parallel, no increase of the PbI_2 related reflections was observed, which signals the formation of either amorphous PbI_2 or that no continuous crystallite domains are formed. Note that the compositions extracted from XRD measurements (majority phase) agree remarkably well with compositions extracted from the UV-vis data (both our own and literature composition – bandgap relation was examined).[4]

XPS data shows a high initial iodide content on the surface of the electrodes (if a stoichiometric methylammonium content is presumed (compositions shown in brackets), an 11

n/n% PbI_2 could be determined). This additional PbI_2 explains the higher than stoichiometric iodide content determined from EDX and ICP-OES + IC measurements respectively. However, as XPS measurements only probe the surface of the samples these data should be generalized with caution. As we perform the electrochemical treatment the surface nitrogen content decreases. With this an initial increase in surface iodide is witnessed, which ultimately decreases as the treatment is finished. This shows the initial enrichment of the surface of the electrodes in iodide and its gradual expulsion towards the electrolyte.

Calculation of average lifetime from transient absorption data

The weighted average lifetime was calculated from the biexponential fits of the recovery traces shown in **Figure 4 A-C**. The parameters obtained from the biexponential fits are shown in **Table S6**, where A_i stands for the amplitude and τ_i stands for the exponent). The formula to calculate the weighted average:

$$\tau_{weighted\ average} = \frac{\sum(A_i\tau_i)^2}{\sum A_i\tau_i} \quad (1)$$

Table S6. Determined lifetimes, from bi-exponential fits carried out on transient absorption data.

	A_1	τ_1 / ps	A_2	τ_2 / ps	τ_{avg} / ps
FTO/$MAPbBr_{3.0}$ - reference	0.48 ± 0.01	104 ± 5	0.50 ± 0.01	1273 ± 59	571 ± 68
FTO/$MAPbBr_{1.5}I_{1.5}$ - before applied bias	0.49 ± 0.01	75 ± 3	0.50 ± 0.01	838 ± 23	381 ± 28
FTO/$MAPbBr_{1.5}I_{1.5}$ - after applied bias	0.37 ± 0.04	49 ± 10	0.56 ± 0.04	4 ± 0.5	16 ± 8

UV-vis spectroscopic determination of expelled iodide

UV-vis spectroscopic measurements of the electrolyte were carried out to follow the iodide expulsion process. The recorded spectra show characteristics of the I_3^- form (two absorption peaks at 298 nm and 364 nm), which is the direct result of Reaction 2. In this the expelled I_2 together with I^- present in the electrolyte (possibly from the slow dissolution of the films) forms I_3^-. A calibration line (**Fig. S11 A,B**) was obtained by plotting the peak absorbance at 364 nm recorded in 0.1 M Bu_4NI containing DCM media, to ensure full conversion of the added I_2 to I_3^-.

$$I_2 + I^- \rightarrow I_3^- \quad (2)$$

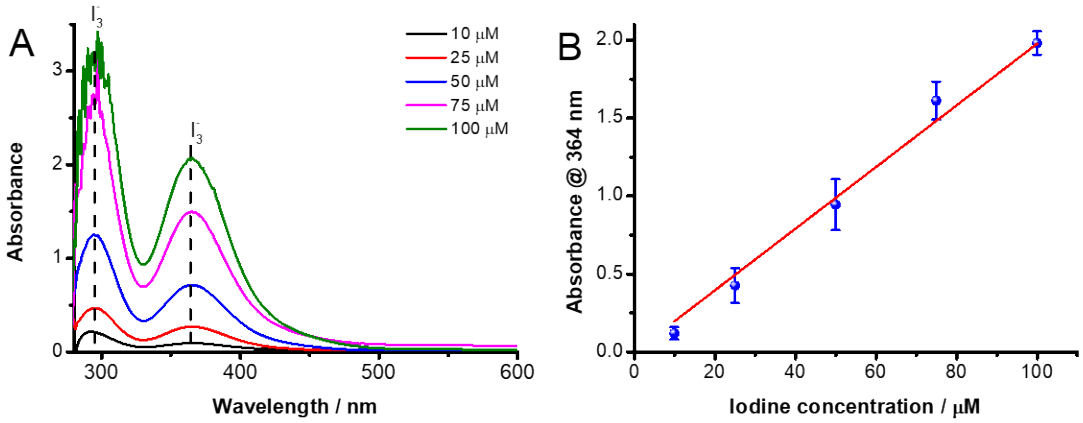

Figure S11. A: UV-vis absorption spectra of varying amount of iodine dissolved in 0.1 M Bu_4NI containing DCM solution. **B:** The determined calibration line for the concentration dependence of the absorbance of triiodide at 364 nm. The standard deviation was determined from three separate sets of measurements

DFT Calculations

Defects calculations have been carried out in periodic boundary conditions in the 2x2x1 tetragonal supercells of $MAPbI_3$ and $MAPbBr_3$. In all cases cell parameters have been fixed to the experimental values, i.e. a=b=8.849 Å, c = 12.642 Å for $MAPbI_3$ [5] and pseudo-cubic cell parameters from Poglitsch a=b=8.345 Å, c = 11.802 Å for $MAPbBr_3$ [6]. Defects equilibrium geometries have been optimized by using the Perdew-Burke_Ernzherof functional (PBE)[7] and ultrasoft pseudopotentials with a cutoff on the wavefunctions of 40 Ryd (320 Ryd on the charge density) and 1x1x2 k-point grids in the Brillouin zone (BZ).

Thermodynamic ionization levels have been calculated at the relaxed PBE structures by performing single point hybrid functional calculations by using the HSE06 functional[8] (exact exchange fraction α=0.43) by including spin-orbit corrections and dispersions interactions a posteriori within the DFT-D3 scheme of Grimme.[9] Calculated ionization levels have been corrected by including potential alignment and Makov-Payne corrections (ionic dielectric constants ε=24.0 and ε=20.0 for $MAPbI_3$ and $MAPbBr_3$, respectively). Hybrid calculations have been performed by using norm conserving pseudopotentials and a cutoff energy on the wavefunctions of 40 Ryd and 1x1x2 k-points in the BZ. All calculations have been carried out by using the Quantum Espresso package.[10]

References

(1) Li, Z.; Mercado, C. C.; Yang, M.; Palay, E.; Zhu, K. Electrochemical Impedance Analysis of Perovskite-Electrolyte Interfaces. *Chem. Commun.* **2017**, *53*, 2467–2470.

(2) Srivastava, P.; Parhi, A. P.; Ranjan, R.; Satapathi, S.; Bag, M. Temperature Assisted Nucleation and Growth To Optimize Perovskite Morphology at Liquid Interface: A Study by Electrochemical Impedance Spectroscopy. *ACS Appl. Energy Mater.* **2018**, *1*, 4420–4425.

(3) Xie, L.-Q.; Zhang, T.-Y.; Chen, L.; Guo, N.; Wang, Y.; Liu, G.-K.; Wang, J.-R.; Zhou, J.-Z.; Yan, J.-W.; Zhao, Y.-X.; et al. Organic–inorganic Interactions of Single Crystalline Organolead Halide Perovskites Studied by Raman Spectroscopy. *Phys. Chem. Chem. Phys.* **2016**, *18*, 18112–18118.

(4) Noh, J. H.; Im, S. H.; Heo, J. H.; Mandal, T. N.; Seok, S. Il. Chemical Management for Colorful, Efficient, and Stable Inorganic–Organic Hybrid Nanostructured Solar Cells. *Nano Lett.* **2013**, *13*, 1764–1769.

(5) Stoumpos, C. C.; Malliakas, C. D.; Kanatzidis, M. G. Semiconducting Tin and Lead Iodide Perovskites with Organic Cations: Phase Transitions, High Mobilities, and Near-Infrared Photoluminescent Properties. *Inorg. Chem.* **2013**, *52*, 9019–9038.

(6) Poglitsch, A.; Weber, D. Dynamic Disorder in Methylammoniumtrihalogenoplumbates (II) Observed by Millimeter-wave Spectroscopy. *J. Chem. Phys.* **1987**, *87*, 6373–6378.

(7) Perdew, J. P.; Burke, K.; Ernzerhof, M. Generalized Gradient Approximation Made Simple. *Phys. Rev. Lett.* **1996**, *77*, 3865–3868.

(8) Heyd, J.; Scuseria, G. E.; Ernzerhof, M. Hybrid Functionals Based on a Screened Coulomb Potential. *J. Chem. Phys.* **2003**, *118*, 8207–8215.

(9) Grimme, S.; Antony, J.; Ehrlich, S.; Krieg, H. A Consistent and Accurate Ab Initio Parametrization of Density Functional Dispersion Correction (DFT-D) for the 94 Elements H-Pu. *J. Chem. Phys.* **2010**, *132*, 154104.

(10) Giannozzi, P.; Baroni, S.; Bonini, N.; Calandra, M.; Car, R.; Cavazzoni, C.; Ceresoli, D.; Chiarotti, G. L.; Cococcioni, M.; Dabo, I.; et al. QUANTUM ESPRESSO: A Modular and Open-Source Software Project for Quantum Simulations of Materials. *J. Phys. Condens. Matter* **2009**, *21*, 395502.